ELSEVIER

Synthetic biology-inspired design of signal-amplifying materials systems

Hanna J. Wagner [1,2,3], Raphael Engesser [3,4], Kathrin Ermes [1,3], Christian Geraths [1,3], Jens Timmer [3,4], Wilfried Weber [1,2,3,*]

[1] Faculty of Biology, University of Freiburg, Schänzlestrasse 1, 79104 Freiburg, Germany
[2] Spemann Graduate School of Biology and Medicine (SGBM), University of Freiburg, Albertstrasse 19a, 79100 Freiburg, Germany
[3] BIOSS – Centre for Biological Signalling Studies, University of Freiburg, Schänzlestrasse 18, 79104 Freiburg, Germany
[4] Institute of Physics, University of Freiburg, Hermann-Herder Strasse 3, 79104 Freiburg, Germany

Synthetic biology applies engineering concepts to build cells that perceive and process information. Examples include cells engineered to perform basic digital or analog computation. These circuits serve as basis for the construction of complex integrated cellular networks that offer manifold applications in fundamental and applied research. Here, we introduce the concept of using design approaches and molecular tools applied in synthetic biology for the construction of interconnected biohybrid materials systems with information processing functionality. We validate this concept by modularly assembling protein and polymer building blocks to generate stimulus-responsive materials. Guided by a quantitative mathematical model, we next interconnect these materials into a materials system that acts as both a signal detector and as an amplifier based on a built-in positive feedback loop. The functionality and versatility of this materials system is demonstrated by the detection of enzymatic activities and drugs. The modular design concept presented here thus represents a blueprint for integrating synthetic biology-inspired information-processing circuits into polymer materials. As integrated sensors and actuators, the resulting smart materials systems could provide novel solutions with broad perspectives in research and development.

Introduction

Synthetic biology applies engineering principles for the rational design of genetic circuits and the reprogramming of living cells to perform desired functions [1–4]. Within this discipline, interchangeable biological building blocks are modularly and predictably assembled to generate synthetic regulatory circuits that confer novel properties to the biological system. Similar to electrical engineering and control theory, the synthetic biological design principle exhibits a hierarchical architecture: basic parts with sensing, switching, or processing functions serve as building blocks for the construction of circuits and devices that can be further interconnected to complex information-processing networks [5].

During the emergence of synthetic biology, a variety of complex genetic circuits have been developed in prokaryotes and eukaryotes, including toggle switches [6,7], hysteretic circuits [8], oscillators [9,10], timing and counting devices [11,12], or cell-to-cell communication systems [13,14]. These cellular devices paved the way for the assembly and implementation of higher-order and application-oriented networks in, for instance, the analytical [15], therapeutic [16], biotechnological [17], energy [18], and environmental [19] sectors. Specific examples include designer cells for the specific detection and ablation of tumor cells [20,21]; regulatory open- and closed-loop circuits

* Corresponding author at: Faculty of Biology, University of Freiburg, Schänzlestrasse 1, 79104 Freiburg, Germany.
E-mail address: Weber, W. (wilfried.weber@biologie.uni-freiburg.de).

 https://doi.org/10.1016/j.mattod.2018.04.006

for the treatment of diabetes [22,23] or diet-induced obesity [24]; and microbial production of chemicals, biologics, and fuels [25]. Similarly, hydrogels have been employed for the spatial or temporal control of engineered cells [26,27], or for enabling the *in vivo* administration of therapeutic cell implants [23,28]. Furthermore, engineered bacterial cells have been used for the formation of 2D and 3D patterns, which have served as basis for the guided assembly of structured materials [29–32].

Synthetic biology thus provides a broad scope and the increase in knowledge, and the development of innovative tools and techniques give reason to expect further creative advances in this field.

Here, we propose the concept that synthetic biological design principles and molecular tools could be extended to materials sciences by following a similar hierarchical assembly approach from modular building blocks to circuits and networks.

Specifically, synthetic biological parts such as sensor and binding proteins, molecular switches, and biocatalysts might not only serve as basis for engineered cellular circuits, but could also offer the possibility to endow materials with novel functions enabling them to perceive external inputs and to react by – for example – transmitting signals to other materials. Similar to synthetic biology, such material-to-material communication systems would lay the foundation for the programming of information-processing materials systems with desired functions.

To demonstrate the validity of this concept, we chose a positive feedback loop configuration. Positive feedback loops are fundamental circuit motifs in electrical engineering and in cell signaling [33–36], and have been widely used in the design of synthetic cellular hysteretic operations [8], oscillators [9,10], analog computation [3], and sensor circuits [37]. Here, we employ this circuit motif to generate signal-amplifying materials systems that detect analytes of interest. We first designed protein building blocks that have sensor, switch, transmitter, or output function. Next, we combined these synthetic biological building blocks with chemical polymers to generate stimulus-responsive materials. Guided by a mathematical model, we interconnected these material units to build information-processing materials circuits that amplify input signals in a forward or positive feedback configuration. We demonstrate that these materials systems can be used to detect biomolecules such as enzymes or drugs. The modular system design offers high flexibility, enabling the interchangeability and customization of the biological building blocks and thus the general design of computing materials systems. We envision that the concept presented here will lay the foundation for the design and generation of synthetic biology-inspired materials systems for diverse applications.

Results and discussion

In this study, we aimed to combine materials sciences with synthetic biology in order to construct information-processing materials systems. To this end, we hierarchically assembled basic biological and polymer parts into a biomaterials-based positive feedback loop, and applied this circuit for analyte detection and signal amplification. Positive feedback-based signal amplification is a recurrent motif in prokaryotic and eukaryotic cell signaling [33–36] and has been exploited for the design of synthetic biological sensor circuits [3,9,37]. Inspired by these cellular blueprints, we aimed to arrange two stimulus-responsive hydrogel materials in a positive feedback loop. In this configuration, the first material senses an external input signal (IN) and transmits the signal to the second material, which in turn further activates the first material in a positive feedback loop and simultaneously triggers the release of a molecule that is measured as the output response (OUT, Fig. 1a).

To generate materials with sensing, transmission, feedback and output functions, we first compiled a toolbox of polymers and basic synthetic biology-derived building blocks (Fig. 1b). The toolbox comprises two proteases tobacco etch virus (TEV) protease and Caspase-3 (Casp3) that specifically cleave their target peptide sequences, TEV cleavage site (TCS) and Casp3 cleavage site (CCS), respectively. Casp3 was engineered to be activatable by a third protease, the human rhinovirus-14 3C protease (3CPRO). This was achieved by replacing the native cleavage site for proteolytic activation in Casp3 by a 3CPRO cleavage site. The proteins were non-covalently coupled to a polymer framework by exploiting binding of the bacterial gyrase subunit B (GyrB) to novobiocin-functionalized crosslinked agarose ($K_d \sim 1–2 \times 10^{-8}$ M [38]), or the binding of hexahistidine-tag (His_6-tag) to Ni^{2+}-nitrilotriacetic acid (Ni^{2+}-NTA)-functionalized polyacrylamide (poly(AAm-co-Ni^{2+}-NTA-AAm) ($K_d \sim 1–2 \times 10^{-8}$ M [39]). For the latter material, mixing a protein functionalized with two His_6-tags with poly(AAm-co-Ni^{2+}-NTA-AAm) results in gelation [40].

The aforementioned building blocks were used to generate the signal-amplifying materials system (Fig. 1a and c). The first material (hereafter referred to as module A) contains TEV immobilized to an agarose polymer network via two CCSs. The second material (module B) harbors the output protein (red fluorescent protein mCherry, OUT) that crosslinks the polymer framework via two TCS-containing His_6 anchors. Additionally, inactive 3CPRO-inducible Casp3 ($Casp3_{OFF}$) is anchored to module B using aTCS-containing linker. The use of this Casp3 variant minimizes unintended system activation and auto-amplification in the absence of the input signal (3CPRO). Furthermore, it converts the binary output (on/off) of the positive feedback loop into an analog output that correlates with the input concentration.

The non-covalent anchoring of the proteins to the polymer frameworks permits the release of low amounts of $Casp_{OFF}$ to support the initiation of the positive feedback loop amplification. Addition of the input signal (3CPRO) triggers the conversion of $Casp3_{OFF}$ to active Casp3 ($Casp3_{ON}$), which subsequently cleaves its CCS substrate to release TEV from module A. Free TEV induces the release of additional $Casp3_{OFF}$ to fuel the positive feedback loop (indicated by arrows with increasing thickness in Fig. 1c). Concurrently, TEV cleaves the TCS anchors of the output protein (mCherry), thereby reducing the crosslinks between the polymer chains to dissolve the hydrogel network and releasing mCherry.

Prior to the assembly of the complete materials system, we characterized each subsystem individually. For synthesis of material module A, we fused the TEV protease to two GyrB domains via Casp3-cleavable CCS linkers and immobilized the fusion

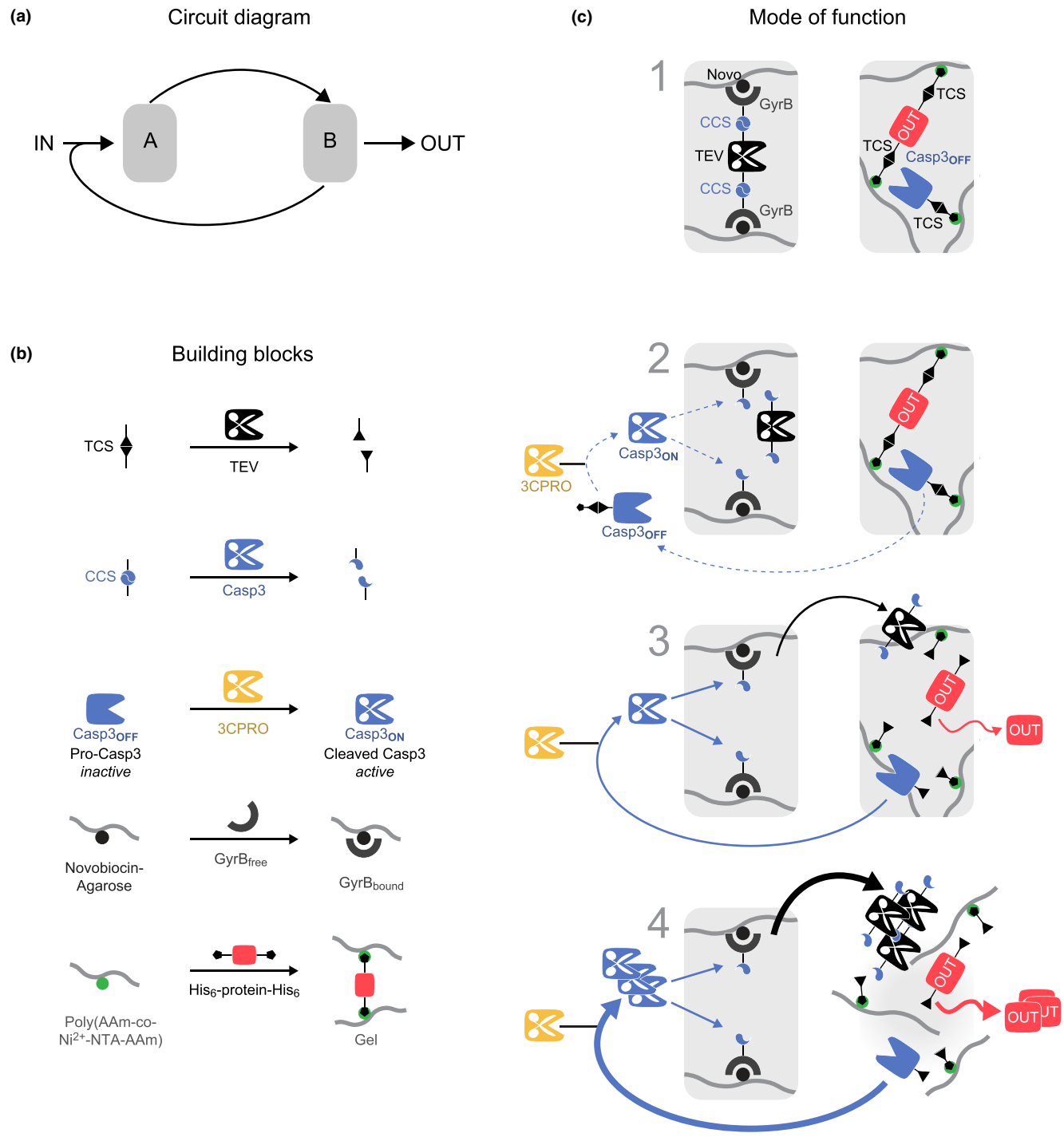

FIGURE 1

Design of the signal amplifying materials system. (a) Circuit diagram. Two modules A and B are wired in a positive feedback configuration controlled by the input signal. (b) Synthetic biology-derived building blocks and chemical polymers used for the construction of the materials systems. The tobacco etch virus (TEV) and Caspase-3 (Casp3) proteases cleave their target sites (TEV cleavage site, TCS, and Casp3 cleavage site, CCS) in a sequence-specific manner. The proteolytic activity of an engineered variant of $Casp3_{OFF}$ can be induced by 3C protease (3CPRO, $Casp3_{ON}$). Protein–polymer binding is achieved by the bacterial DNA gyrase subunit B (GyrB) binding to novobiocin-coupled crosslinked agarose or by a hexahistidine (His_6)-tag binding to Ni^{2+}-nitrilotriacetic acid (NTA)-functionalized polyacrylamide (poly(AAm-co-Ni^{2+}-NTA-AAm). The latter is crosslinked to a hydrogel by adding a double His_6-tagged protein. (c) Molecular design and mode of function of the signal-amplifying materials system. Module A is composed of TEV bound to novobiocin (Novo)-functionalized polymer via two GyrB domains. Both linker regions between TEV and GyrB contain Casp3-sensitive CCS sequences. Material module B comprises Ni^{2+}-NTA functionalized-polyacrylamide that is crosslinked via two His_6-tagged TCS linkers of the output protein (OUT). $Casp3_{OFF}$ is immobilized within this module by a His_6-tagged TCS linker. Low $Casp3_{OFF}$ amounts that are released due to the non-covalent nature of the Ni^{2+}-NTA/His_6-tag interaction (dashed blue line) are activated by the input signal, 3CPRO (step 2). Activated Casp3 ($Casp3_{ON}$) cleaves CCS and triggers the release of TEV (step 3). Free TEV cleaves its target sites in OUT and Casp3, thereby enhancing Casp3 release and further fueling the feedback loop (step 4). The gray lines represent the polymer network, the black and green dots the protein-polymer attachment sites as described in (b).

protein on novobiocin-functionalized, crosslinked agarose (Fig. 2a). We subsequently evaluated the Casp3-mediated release of TEV from the resulting material (Fig. 2b). Quantification of TEV activity in the supernatant revealed that release of TEV from the material was dependent on Casp3 concentration (Fig. 2b). Next, we synthesized material module B by crosslinking poly (AAm-co-Ni^{2+}-NTA-AAm) with a protein linker comprising two Ni^{2+}-binding His_6-tags and TCSs flanking the output protein mCherry. The resulting hydrogel should therefore undergo gel-to-sol transition upon the addition of free TEV, which cleaves the TCS of the crosslinking protein (Fig. 3a). Indeed, increasing concentrations of TEV resulted in a dose-dependent dissolution of the hydrogel as monitored by the release of fluorescent mCherry (Fig. 3b). In module B we incorporated a 3CPRO-activatable Casp3, which was coupled to the matrix via a linker containing a His_6-tag and a TCS (Fig. 3c). We tested the functionality of this construct in the presence or absence of the initiator protease 3CPRO. SDS–PAGE analysis confirmed cleavage of the Casp3 construct by 3CPRO (Fig. 3d), which correlated with induction of Casp3 proteolytic activity (Fig. 3e).

After confirming the functionality of each subsystem, we assembled the complete signal-amplifying materials system. To this end, we applied an iterative approach following a design – build – test cycle supported by mathematical model-based predictions of optimized system functionality. We chose a system volume of 1.5 mL, enabling easy handling of all components while still being small enough to be in the range of portable devices.

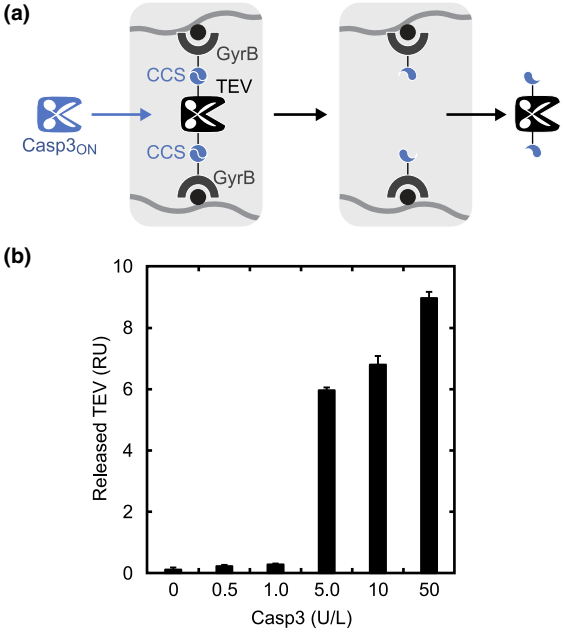

FIGURE 2

Design and characterization of material module A. (a) Design of module A. The TEV protease is flanked by two GyrB domains for immobilization to novobiocin-functionalized agarose. The linkers between GyrB and TEV contain Casp3 cleavage sites (CCSs). In the presence of Casp3, CCS is processed and TEV is released. (b) Casp3 concentration-dependent release of TEV from material module A. 3.4 mg of crosslinked Sepharose was functionalized with novobiocin for the immobilization of the TEV fusion construct. The material was incubated with the indicated concentrations of Casp3 and 5 μg 3CPRO for Casp3 activation in a total volume of 300 μL for 6 h at RT with agitation. The release of TEV was determined by measuring its activity in the supernatant. Mean values ± s.e.m. of four replicates are shown.

First, we assembled the basic feedback circuit as depicted in Figs. 1c and 4a. When both material modules were combined, addition of increasing 3CPRO concentrations correlated with increased dissolution rates of module B, thus confirming the functionality of the positive feedback loop (Fig. 4b). However, the system response was rather slow, reaching 50% dissolution of module B only after 42 h in the presence of high 3CPRO concentrations (0.7 μg mL^{-1}). Therefore, we aimed to rationally design alternative configurations with faster response characteristics. In order to predict the effect of design variations on the system's performance, we developed a quantitative ordinary differential equation-based mathematical model (see Supplementary information for the derivation of the model). The model kinetic parameters were inferred from experimental data of the basic feedback system (see Figs. 1 and 2 in Ref. [41]). We hypothesized that the time required for activation of Casp3, actuation of the feedback loop, and hence accumulation of Casp3 at module A might be critical for the system's kinetics, and that a shortcut directly driving the release of TEV in a Casp3-independent manner could accelerate the system. We evaluated how a direct 3CPRO-mediated release of TEV would amplify the input in a forward configuration by means of a two-step proteolytic cascade (3CPRO-triggered release of TEV, followed by TEV-dependent dissolution of material module B and release of mCherry output signal, Fig. 4c). Simulations of the time required for 50% dissolution of module B as a function of the 3CPRO concentration and the 3CPRO-mediated release of TEV revealed that the forward amplification configuration could effectively accelerate the system's response compared to the positive feedback loop alone (Fig. 4d, area above red-dotted line). Based on these predictions, we constructed a modified materials system in which TEV was coupled to the polymer framework in module A via a tandem linker consisting of a 3CPRO cleavage site (3CS) and CCS (see Fig. 3 in Ref. [41] for characterization). We combined this modified module A with module B lacking Casp3 to solely analyze the forward amplification (Fig. 4c). Indeed, with 3CPRO input concentrations comparable to those used before, this forward amplification reached half-maximal hydrogel dissolution in less than 20 h after addition of 3CPRO (Fig. 4e).

In addition to speeding up the system, we aimed to enhance its sensitivity to low input concentrations of 3CPRO. We hypothesized that a combination of the forward (Fig. 4c) and the positive feedback loop (Fig. 4a) amplification would result in both faster response and higher sensitivity, and that this could be achieved by combining module A from the forward amplification system with $Casp3_{OFF}$-containing module B from the basic feedback loop system (Fig. 4f). To test this hypothesis, we implemented this design in the mathematical model and inferred parameters from experimental data (see Figs. 2 and 4 in Ref. [41]). As measure for sensitivity, we used the area between the response curves (dissolution time-courses) obtained in the absence and presence of the lowest concentration of 3CPRO (green area in Fig. 4e). As shown in Fig. 4g, accelerating

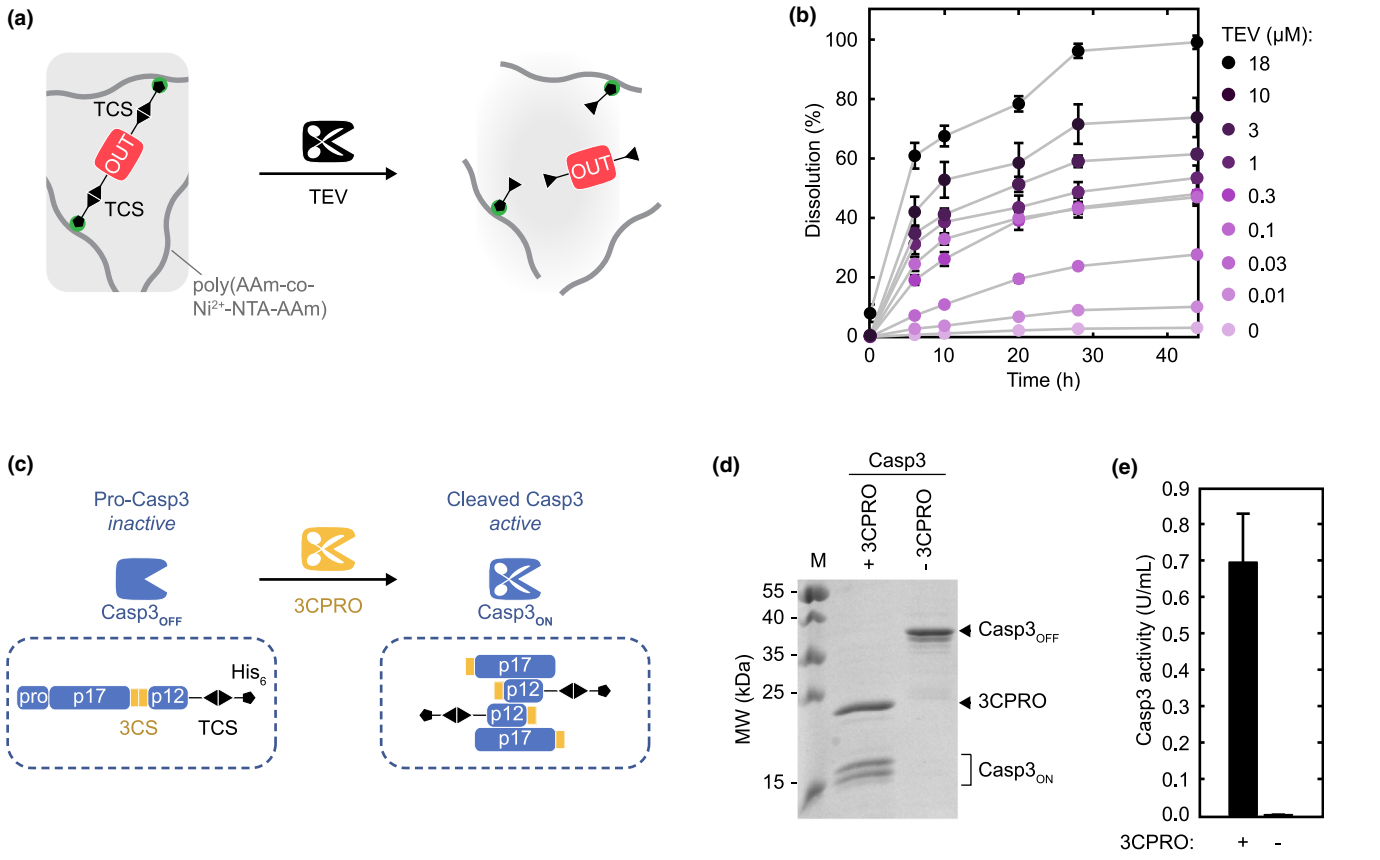

FIGURE 3

Design and characterization of material module B. (a) Design of module B. The output protein (OUT) red fluorescent protein mCherry was amino- and carboxy-terminally fused to TEV cleavage site (TCS)-containing linkers and His_6-tags. The polymer (poly(AAm-co-Ni^{2+}-NTA-AAm)) was crosslinked by the Ni^{2+}-NTA/His_6-tag interaction between polymer and crosslinking output protein. In the presence of TEV protease the crosslinking protein is cleaved, resulting in hydrogel dissolution and release of fluorescent output protein. (b) Dissolution characteristics of the output hydrogel in response to TEV protease. Hydrogels were incubated with the indicated concentrations of TEV protease and the dissolution was monitored by quantifying the fluorescence of released mCherry. Mean values of eight replicates ± s.e.m. are shown. (c) Design of 3CPRO-inducible Casp3. The endogenous cleavage site between large (p17) and small (p12) subunit was replaced with the cleavage site for 3CPRO (3CS, yellow). A TCS-linker and His_6-tag were fused to the carboxy-terminus. Cleavage of Casp3 by 3CPRO leads to the formation of the active, heterotetrameric form of Casp3 ($Casp3_{ON}$). (d) 3CPRO-mediated processing of activatable Casp3. 13 μg 3CPRO-inducible Casp3 were incubated with 5 μg 3CPRO. Cleavage products were analyzed by SDS–PAGE. (e) 3CPRO-mediated activation of Casp3. The activity of cleaved and non-cleaved Casp3 was determined by a colorimetric Casp3 assay. Mean values ± s.e.m. of three replicates are shown.

the release kinetics of TEV achieved by combining both systems was predicted to result in an increased sensitivity (area between the curves) at 3CPRO input concentrations below 0.03 μg mL^{-1}. Experimental implementation revealed that the system's response to the lowest 3CPRO input concentration (0.006 μg mL^{-1}) was doubled as compared to the sole forward wiring of the materials (indicated by the green areas between the curves, see Fig. 4e, h and Fig. 4 in Ref. [41] for comparison). These data validate the model-based predictions and further demonstrate that the modular, model-guided approach allows the rational and predictive design of materials systems with desired information-processing functionality.

Due to its modular design, this signal-amplifying materials system could be applied as generic sensor for proteases by exchanging 3CS with the cleavage motif of other target proteases. We next evaluated whether such materials systems could also be applied for the detection of small molecular analytes such as metabolites or drugs. As a model compound we chose the aminocoumarin antibiotic novobiocin (Albamycin™), which is licensed for human and veterinary use (including lactating dairy cattle) [42]. To render the system responsive to novobiocin, we introduced a third module in which the previous input, 3CPRO, was immobilized to novobiocin-functionalized crosslinked agarose via the novobiocin-binding protein GyrB (Fig. 5a). In this configuration, the addition of free novobiocin competes with immobilized novobiocin for the binding to GyrB, thus triggering the release of 3CPRO (Fig. 5a and b). Furthermore, free novobiocin triggers the release of TEV from material module A by binding to GyrB used to anchor TEV protease to the novobiocin-functionalized polymer framework (Figs. 1c, 5c and d). In order to experimentally demonstrate the detection of novobiocin, we combined the novobiocin-sensitive 3CPRO-containing module (Fig. 5a) with modules A and B (Fig. 4a) of the basic feedback loop as depicted in Fig. 5e. Addition of free novobiocin is expected to release both TEV and 3CPRO to initiate forward signal propagation and to activate free $Casp3_{OFF}$ for positive feedback loop amplification, respectively. Indeed, we showed that the dissolution rate of

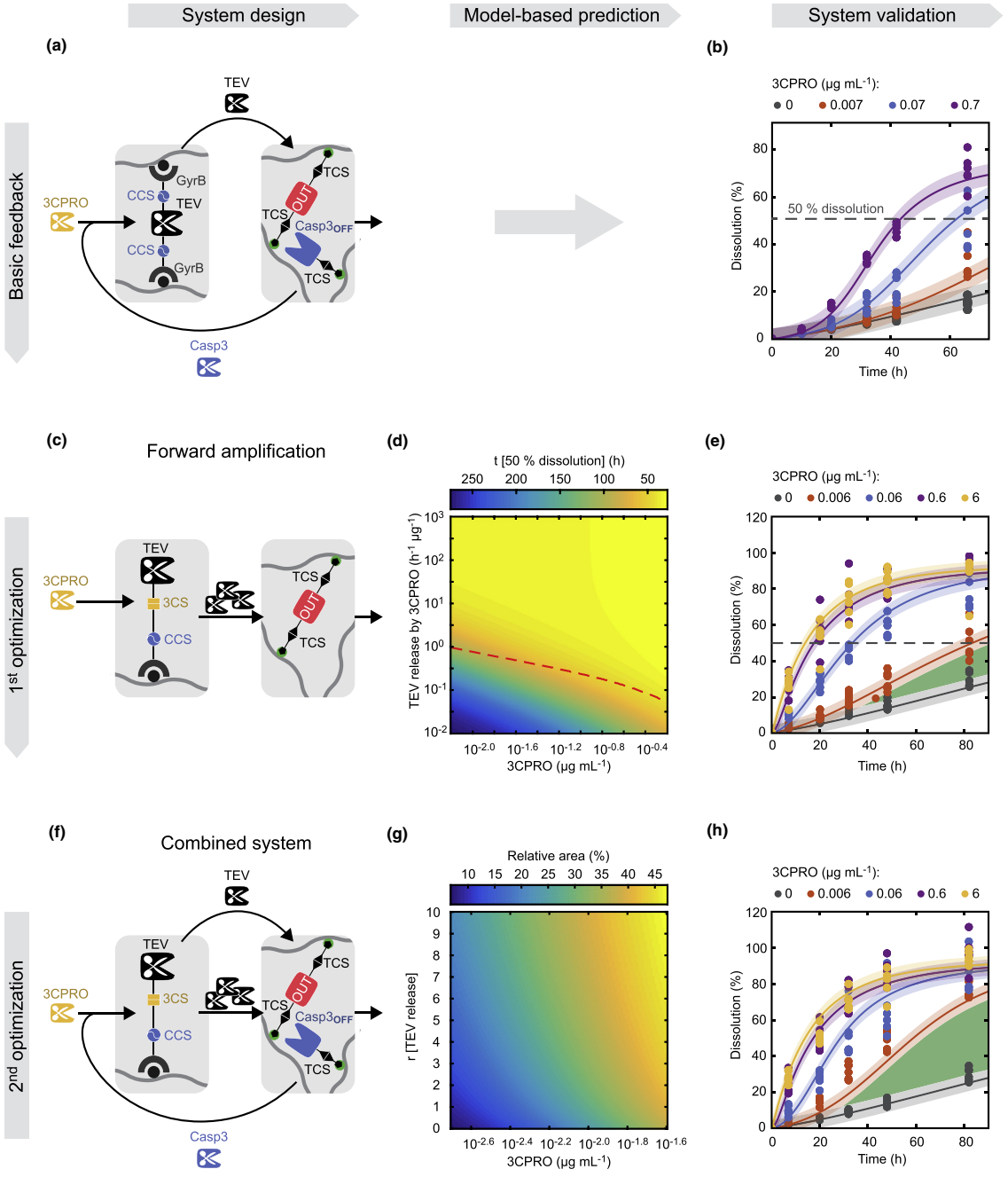

FIGURE 4

Implementation of the signal-amplifying materials system for the detection of 3CPRO protease activity. (a and b) Design and characterization of the basic positive feedback materials system (see also Fig. 1c). Module B was synthesized incorporating 0.015 U Casp3 and combined with material module A containing 2 RU TEV. Dissolution of module B upon addition of the indicated amounts of 3CPRO was monitored by quantifying the fluorescence of released mCherry. (c) Implementation of a materials system with forward signal amplification. TEV was immobilized via a 3CPRO cleavage site (3CS)-containing anchor within the material thereby enabling a direct 3CPRO-mediated release of TEV. Module B was synthesized as in (a) but without Casp3. (d) Model prediction of the performance of a forward amplification system assuming a direct 3CPRO-mediated release of active TEV. Shown is the time required for 50% hydrogel dissolution (color code) as a function of 3CPRO amounts and velocity rate constants of 3CPRO-mediated release of TEV. The area above the red dashed line indicates the conditions under which the forward amplification system shows a faster response compared to the basic feedback system. (e) Characterization of the forward signal amplification system. Material module A (1.6 RU TEV) was combined with hydrogel module B (without Casp3). The system response as a function of 3CPRO input was quantified by monitoring module B dissolution via released mCherry. (f) Design of the optimized signal amplifying materials system. Material module A of the forward amplification system (c) was combined with module B of the basic feedback system (a). 3CPRO triggers the release of TEV (forward amplification) and activates $Casp3_{OFF}$ (feedback amplification). (g) Heat map showing the model prediction of the sensitivity to low 3CPRO input concentrations as a function of the rate of Casp3-induced release of TEV (r[TEV release], relative rate compared to the basic feedback system). As a measure for sensitivity, the area between the curves corresponding to the dissolution kinetics in the absence and presence of indicated 3CPRO amounts was used, highlighted in (e) and (h) as green areas. (h) Characterization of the optimized signal-amplifying materials system. Material module A (1.6 RU TEV) was assembled with module B (containing 0.015 U Casp3). The dissolution of module B in the presence of indicated 3CPRO amounts was monitored by quantifying released mCherry. The curves in (b), (e), (h) represent the model fits. The shaded error bands correspond to one standard deviation.

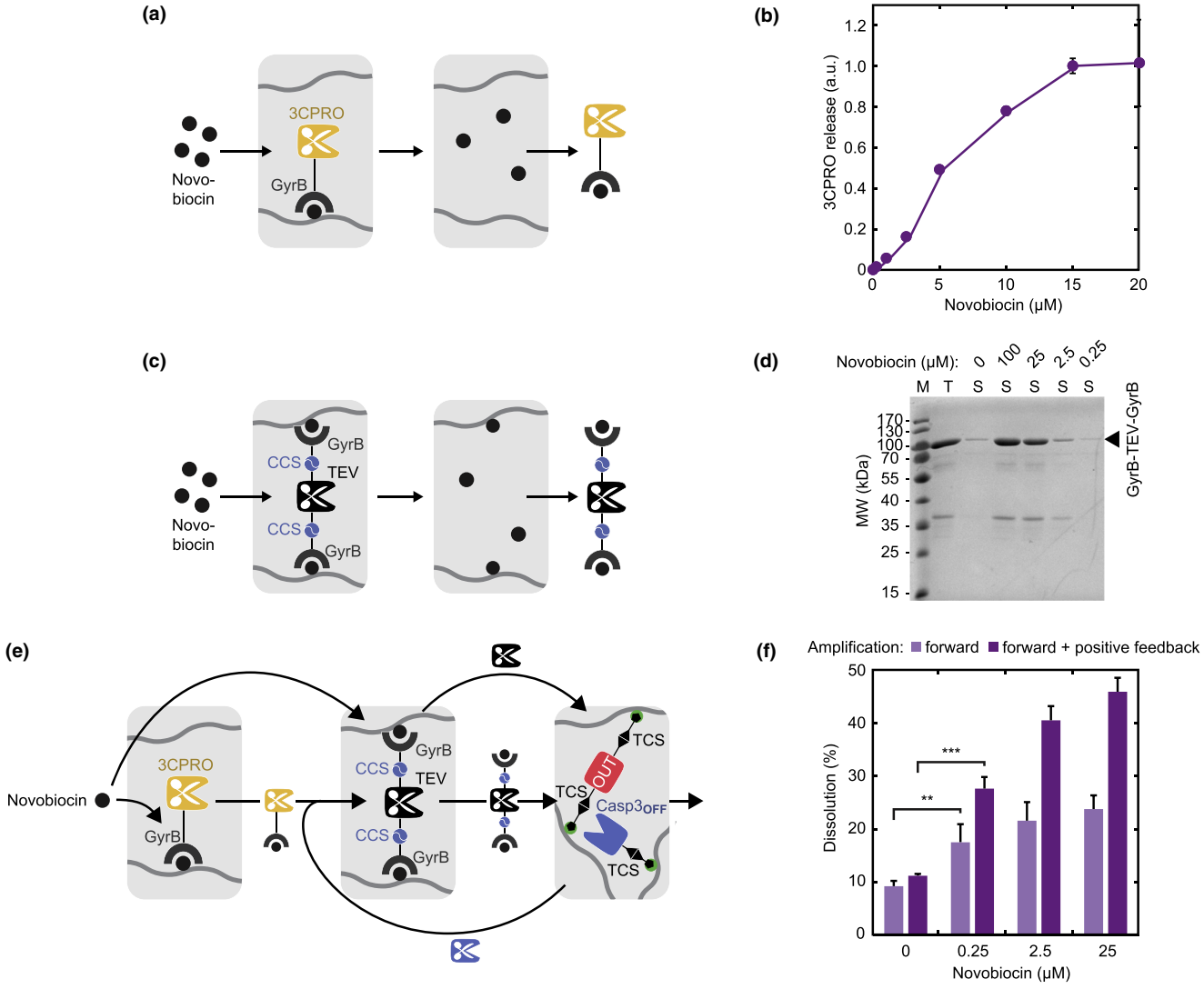

FIGURE 5

Modular extension for the detection of novobiocin by the signal amplifying materials system. (a) Design of the novobiocin-sensing module. 3CPRO is fused to GyrB, which binds to novobiocin-functionalized agarose. Addition of free novobiocin competes with bound novobiocin for GyrB and releases 3CPRO from the material. (b) Characterization of novobiocin-responsive 3CPRO release. 3CPRO was immobilized on novobiocin-agarose (1.2 mg/sample) and incubated with the indicated novobiocin concentrations for 2 h at room temperature. The supernatants were collected and released 3CPRO was quantified. Values were normalized to the maximum signal of released protein. Mean values ± s.e.m. of three replicates are shown. (c) Novobiocin-triggered release of TEV. In module A, addition of free novobiocin releases TEV by competing for binding to GyrB. (d) Novobiocin-mediated release of TEV from material module A. The same experimental setup as described in Fig. 2b was used. Instead of adding Casp3, the indicated concentrations of novobiocin were added. SDS–PAGE of free (S, supernatant) and total (T) protein was conducted to evaluate the novobiocin-triggered release of TEV protease. (e) Design of the materials system for the detection of novobiocin. The 3CPRO-containing material (a) was combined with materials from the basic feedback loop system (Figs. 1c and 4a). Addition of free novobiocin triggers the release of 3CPRO and TEV. Released TEV mediates the dissolution of module B (forward amplification). Concurrently, released 3CPRO activates Casp3 and thereby enhances the release of TEV (feedback amplification). (f) Experimental characterization of the materials system for the detection of novobiocin. The materials system shown in e was implemented with 0.005 U Casp3, 1.5 RU TEV and 7.5 μU 3CPRO. The system was exposed to the indicated novobiocin concentrations and the output was measured after 49 h (dark purple bars). As control, the system was implemented and characterized without Casp3 resulting in forward amplification only (light purple bars). Mean values of six replicates ± s.e.m. are shown. Statistical analysis: unpaired *t*-test with Welch's correction, $^{**}p < 0.01$, $^{***}p < 0.001$.

module B correlated with the novobiocin input concentration (Fig. 5f). In control experiments relying on forward amplification only (omission of Casp3 in module B), we observed less efficient dissolution (Fig. 5f and see Fig. 5 in Ref. [41] for detailed characterization of the system), which supports the role of the positive feedback loop for signal amplification. These results demonstrate that the signal amplifying materials system is suitable for the detection of novobiocin in the range of the maximum residue limit in milk set by the US Food and Drug Administration (0.1 μg mL^{-1}). The obtained data highlight the versatility of the materials system design for the detection of proteolytic enzymes or small molecules. The modular design suggests that the system could be applied for the detection of analytes beyond those demonstrated in this work by

exchanging the GyrB–novobiocin pair with other ligand–receptor combinations.

Inspired by molecular tools and design concepts derived from synthetic biology, we developed and validated a concept for the design of materials systems with computational functionality. Synthetic biology emerged with the model-guided design of genetic networks with computational capacity, first in bacteria [43], then in higher eukaryotes such as mammalian cells [44]. Although these pioneering studies did not directly demonstrate specific applications of these synthetic networks, the underlying design concepts they introduced were crucial for the rapid expansion of synthetic biology and the development of applications that now provide novel solutions along the value creation chains in various sectors. In this study, we presented the concept of synthesizing materials systems with computational functionality similar to that of the original synthetic biological networks. To demonstrate an early application potential of our design concept, we developed a materials system for the sensitive detection of hydrolytic enzymatic activities and of ligand–receptor interactions. Both functionalities are recurrent in different analytical, drug discovery, or diagnostic applications. Combination of these conceptual principles with the multitude of available synthetic biological modules and circuits could enable the development of materials that perform diverse and complex computations. Materials systems that distinguish multiple environmental cues, process this information, and produce differentiated outputs could act as autonomous and smart multi-input sensors and actuators and inspire the development of manifold applications in the biomedical, analytical and engineering sectors.

Materials and methods

Materials

LB medium, ampicillin sodium salt, isopropyl β-D-1-thiogalactopyranoside (IPTG), novobiocin sodium salt, ethylenediamine tetraacetic acid disodium salt dihydrate, and transparent 96-well, flat-bottom plates were purchased from Carl Roth GmbH. Chloramphenicol was obtained from AppliChem. 2-mercaptoethanol (2-ME), bovine serum albumin (BSA), and Sigmacote were purchased from Sigma–Aldrich. Ni-NTA agarose was purchased from QIAGEN. SnakeSkin dialysis tubing (3.5 k MWCO) and Pierce dextran desalting columns (5k MWCO, 5 mL) were purchased from Thermo Fisher. Protein assay dye reagent concentrate was obtained from Bio-Rad. Epoxy-activated Sepharose 6B was purchased from GE Healthcare Life Sciences. Spin-X UF 6 Concentrators (10 k MWCO) and black 96-well plates were obtained from Corning. The SensoLyte 520 TEV Activity Assay Kit was purchased from AnaSpec. The Colorimetric HRV 3C Protease Activity Assay Kit and the Caspase-3 Colorimetric Assay Kit were purchased from BioVision. Bacterial cells were disrupted using a Bandelin Sonoplus HD 3100 homogenizer. Fluorescence measurements were conducted using an Infinite M200 pro microplate reader (Tecan). Gel permeation chromatography (GPC) was conducted with a 1260 Infinity LC-System (Agilent) using a Suprema three-column system (pre-column, 1000 Å, 30 Å; 5-μm particle size; PSS).

Plasmids

The design and cloning of all plasmids used in this study are described in Tables 3 and 4 in Ref. [41].

Protein production and purification

All recombinant proteins were produced in BL21(DE3)pLysS *E. coli* (Invitrogen). Bacteria were grown in shake flasks containing 1 L LB medium supplemented with 100 μg mL^{-1} ampicillin and 36 μg mL^{-1} chloramphenicol. At OD_{600} = 0.6 protein production was induced with 1 mM IPTG for 4 h at 37 °C, except for TEV (HJW53 and HJW177), which was produced at 30 °C. Cells were harvested at 6000×*g* for 10 min, resuspended in Ni lysis buffer (50 mM NaH_2PO_4, 300 mM NaCl, 10 mM imidazole, pH 8.0), and disrupted by sonication (with 60% amplitude and 0.5 s/1 s pulse/pause intervals). The crude lysates were centrifuged at 30,000 × *g* for 30 min and the proteins were purified by immobilized metal affinity chromatography (IMAC) using Ni-NTA agarose. After removing unbound protein with Ni wash buffer (50 mM NaH_2PO_4, 300 mM NaCl, 20 mM imidazole, pH 8.0), the proteins were eluted with Ni elution buffer (50 mM NaH_2PO_4, 300 mM NaCl, 250 mM imidazole, pH 8.0). Purified TEV (HJW53 and HJW177) and Casp3 (HJW181) were supplemented with 5 mM 2-ME. The crosslinking output protein (HJW2) and the 3CPRO inducer (HJW4) were dialyzed against imidazole-free Ni lysis buffer using a SnakeSkin dialysis tubing with 3.5k MWCO at 4 °C. Buffer exchange for the Casp3 construct (HJW181) into hydrogel buffer (imidazole-free lysis buffer, supplemented with 5 mM 2-ME) was conducted using a dextran desalting column (5k MWCO, 5 mL). The protein concentrations were determined by Bradford assay.

Synthesis of TEV- (module A) and 3CPRO-containing materials

The TEV- and 3CPRO-containing materials were synthesized by functionalizing epoxy-activated Sepharose 6B with novobiocin based on a modified protocol described previously [45]. Briefly, epoxy-activated material was suspended in water and incubated for 30 min at RT. After washing with 200 mL water per gram Sepharose and equilibration with coupling buffer (0.3 M sodium carbonate–bicarbonate buffer, pH 9.5), the material was resuspended in coupling buffer containing 200 mM novobiocin (4.4 mL novobiocin solution per gram material) and incubated at 37 °C for 16 h with shaking. Excess novobiocin was removed by washing with coupling buffer and non-reacted epoxy-groups were blocked by incubation in 1 M ethanolamine, pH 8.5, at 37 °C for 4 h, shaking. The novobiocin-coupled Sepharose was washed with coupling buffer, followed by three cycles of alternating washing steps with water, buffer A (0.1 M Tris/HCl, 0.5 M NaCl, pH 8.0), water, buffer B (0.1 M acetate buffer, 0.5 M NaCl, pH 4.0). To prevent unspecific protein adsorption, the novobiocin-coupled material was blocked with 1% (w/v) BSA in phosphate-buffered saline (PBS) overnight at 4 °C with agitation.

To determine its binding capacity, the resulting material (corresponding to 0–9.0 mg of epoxy-activated Sepharose) was incubated with 0.5 nmol GyrB–mEGFP–3CPRO at 4 °C for 7.5 h, rotating. The amount of unbound protein in the supernatant was determined by measuring the fluorescence of mEGFP at 490/520 nm Ex/Em. As depicted in Fig. 6 in Ref. [41], 3 mg

material bound >90% of protein, indicating a degree of functionalization of 0.17 nmol per gram of epoxy-activated Sepharose.

For further experiments, an excess of GyrB-fused TEV or 3CPRO constructs (1.12 nmol per gram of epoxy-activated Sepharose) was used, ensuring maximal functionalization of the novobiocin–Sepharose. To allow binding, the protein/material mix was incubated in hydrogel buffer supplemented with 10% (v/v) glycerol and 0.1% (w/v) BSA overnight at 4 °C with agitation.

Synthesis of material module B

For module B, Ni^{2+}-charged poly(acrylamide-co-NTA-acrylamide) (poly(AAm-co-Ni^{2+}-NTA-AAm)) was synthesized using one NTA-AAm group per four acrylamide monomers, as described previously by Ehrbar et al. [46]. We determined the average molecular weight (M_n) and polydispersity index (PDI) of synthesized poly(AAm-co-Ni^{2+}-NTA-AAm)) by GPC. For this, a stock solution of 3.33 mg mL^{-1} copolymer was prepared in Ni elution buffer supplemented with 0.05% (w/v) NaN_3 and filtered through a 0.45-μm syringe filter. Subsequently, 0.4 ml of stock solution was injected in the port of the GPC device. Chromatography was performed at a constant flow rate of 0.5 ml min^{-1} in Ni elution buffer. Copolymer samples were separated on a Suprema three-column system, which was placed in an external column oven at 55 °C. Gradient copolymers were analyzed by refractive index (RI) and UV detectors. A calibration curve (10 points) was established using a pullulan standard. With reference to this standard, a M_n of 439.77 kDa with a PDI of 1.993 was estimated.

The crosslinking protein was concentrated using a Spin-X UF 6 Concentrator 10 k MWCO. For the synthesis of a typical hydrogel, 750 μg crosslinking protein was mixed with 0–0.015 U Casp3 in 15 μL hydrogel buffer. Subsequently, the protein solution was mixed with 10 μL 1.8% (w/v) poly(AAm-co-Ni^{2+}-NTA-AAm) on a siliconized (Sigmacote) glass slide. The hydrogels were incubated in a humidified atmosphere overnight at RT. To remove non-bound protein, the gels were incubated in hydrogel buffer for 6 h at RT. The hydrogels were transferred to fresh hydrogel buffer and incubated overnight at RT.

Materials system assembly

Prior to assembling the complete feedback materials system, the TEV- and/or 3CPRO-containing materials were washed with hydrogel buffer supplemented with 0.1% (w/v) BSA and 10% (v/v) glycerol. An equal amount of novobiocin-Sepharose was added and activities of TEV or 3CPRO were determined (see Section Analytical methods). 3CPRO- and/or TEV-functionalized Sepharose were combined with one hydrogel in 1.5 mL hydrogel buffer, supplemented with 10% (v/v) glycerol. 10 μL of indicated amounts of inducer (3CPRO or novobiocin) were added. The dissolution of the hydrogel at RT and with gentle agitation was monitored over time by determining the release of the output protein mCherry. At the end of the time series, the hydrogels were fully dissolved by the addition of 25 mM EDTA. The mCherry fluorescence of fully dissolved gels was used for normalization (100% dissolution).

Analytical methods

Sodium dodecyl sulfate (SDS) polyacrylamide gel electrophoresis (SDS–PAGE, 12% (w/v) gels) with subsequent Coomassie brilliant blue staining was conducted to evaluate the release and/or cleavage of constructs. For monitoring the release, released (S, supernatant) and total (T, supernatant and material-bound protein released during boiling of the material samples in SDS loading buffer) protein was analyzed. The dissolution of hydrogels was determined by measuring the fluorescence of released mCherry in black 96-well plates (excitation: 575 nm, emission: 620 nm). The release of GyrB–mEGFP–3CPRO was analyzed by measuring the fluorescence of the material supernatant (excitation: 490 nm, emission: 520 nm). TEV activity was determined using the SensoLyte 520 TEV Activity Assay Kit according to the manufacturer's protocol with the following changes: 25 μL TEV containing buffer were mixed with 25 μL substrate solution in black 96-well plates and the increase in fluorescence was recorded (excitation: 490 nm, emission: 520 nm). A dilution series of 5-FAM (0–250 nM in assay buffer, supplemented with TEV substrate, 50 μL per well) was used as calibration standard. For TEV, 1 RU corresponded to the amount of protease that cleaved the substrate amount equivalent to the fluorescence of 1 pmol 5-FAM per min under the assay conditions.

3CPRO activity was measured in transparent 96-well plates using the HRV 3C Protease Activity Assay Kit. 50 μL 3CPRO containing buffer were mixed with 2.5 μL substrate and the increase in absorbance at 405 nm was measured every minute. A dilution series of *p*-nitroaniline (0–500 μM in assay buffer) was used for calibration. For determining Casp3 activity (HJW181), its enzymatic activity was activated overnight by incubating 15 μg Casp3 with or without 5 μg 3CPRO (HJW4) in a total volume of 50 μL hydrogel buffer. Casp3 activity was determined using the Caspase-3 Colorimetric Assay Kit. Activated and control (non-activated) Casp3 were diluted 1:100 in hydrogel buffer and 30 μL were combined with 30 μL 2× reaction buffer (containing 10 mM DTT) and 3 μL 4 mM DEVD-pNA substrate in a transparent 96-well plate. The increase in absorbance at 405 nm was measured every minute. A dilution series of *p*-nitroaniline (0–500 μM in assay buffer) was used for calibration. For Casp3 and 3CPRO, 1 U corresponded to the amount of protease that cleaved 1 μmol of substrate per min under the assay conditions.

The dissolution of hydrogels was normalized to the fluorescence value measured after complete dissolution of the material (=100% dissolution). The release of 3CPRO from module C (Fig. 5b) was normalized to the highest mean value of released 3CPRO.

Statistics

Mean values are shown for at least triplicates with error bars representing ± s.e.m. Statistical significance of the novobiocin detection system was analyzed by unpaired *t*-test with Welch's correction using GraphPad Prism 7; $^{*}p < 0.05$, $^{**}p < 0.01$, $^{***}p < 0.001$.

Declaration of conflicts of interest

None.

Acknowledgments

We thank N. Sprossmann and F. Bartels-Burgahn for technical support, and Christina Groß and S.L. Samodelov for critically reading the manuscript. This work was supported by the European Research Council [FP7/2007-2013]/ERC [259043]-CompBioMat and the excellence initiative of the German Federal and State Governments [EXC-294-BIOSS, GSC-4-SGBM].

Appendix A. Supplementary data

Supplementary data associated with this article can be found, in the online version, at https://doi.org/10.1016/j.mattod.2018.04.006.

References

[1] A.A. Green et al., Nature 548 (2017) 117–121.
[2] J.R. Rubens, G. Selvaggio, T.K. Lu, Nat. Commun. 7 (2016) 1–10.
[3] R. Daniel et al., Nature 497 (2013) 619–623.
[4] J.A.N. Brophy, C.A. Voigt, Nat. Methods 11 (2014) 508–520.
[5] A.L. Slusarczyk, A. Lin, R. Weiss, Nat. Rev. Genet. 13 (2012) 406–420.
[6] T.S. Gardner, C.R. Cantor, J.J. Collins, Nature 403 (2000) 339–342.
[7] B.P. Kramer et al., Nat. Biotechnol. 22 (2004) 867–870.
[8] B.P. Kramer, M. Fussenegger, Proc. Natl. Acad. Sci. U.S.A. 102 (2005) 9517–9522.
[9] J. Stricker et al., Nature 456 (2008) 516–519.
[10] M. Tigges et al., Nature 457 (2009) 309–312.
[11] W. Weber et al., Proc. Natl. Acad. Sci. U.S.A. 104 (2007) 2643–2648.
[12] A.E. Friedland et al., Science 324 (2009) 1199–1202.
[13] L. You et al., Nature 428 (2004) 868–871.
[14] T. Bulter et al., Proc. Natl. Acad. Sci. U.S.A. 101 (2004) 2299–2304.
[15] K. Pardee et al., Cell 159 (2014) 940–954.
[16] W. Weber, M. Fussenegger, Nat. Rev. Genet. 13 (2012) 21–35.
[17] J. Nielsen, J.D. Keasling, Cell 164 (2016) 1185–1197.
[18] P.P. Peralta-Yahya et al., Nature 488 (2012) 320–328.
[19] A. Prindle et al., Nature 481 (2011) 39–44.
[20] K.T. Roybal et al., Cell 164 (2016) 770–779.
[21] Z. Xie et al., Science 333 (2011) 1307–1311.
[22] H. Ye et al., Science 332 (2011) 1565–1568.
[23] M. Xie et al., Science 354 (2016) 1296–1301.
[24] K. Rössger, G. Charpin-El Hamri, M. Fussenegger, Nat. Commun. 4 (2013) 1–9.
[25] S. Ausländer, D. Ausländer, M. Fussenegger, Angew. Chem., Int. Ed. 56 (2017) 6396–6419.
[26] T.L. Deans et al., Proc. Natl. Acad. Sci. U.S.A. 109 (2012) 15217–15222.
[27] Y. Liu et al., Sci. Eng. 1 (2015) 320–328.
[28] H. Ye et al., Nat. Biomed. Eng. 1 (2016) 5.
[29] Y. Cao et al., Nat. Biotechnol. 35 (2017) 1087–1093.
[30] X. Wang et al., Adv. Mater. (2018) 1–10, https://doi.org/10.1002/adma.201705968.
[31] P.Q. Nguyen et al., Adv. Mater. (2018) 1–34, https://doi.org/10.1002/adma.201704847.
[32] A.Y. Chen et al., ACS Synth. Biol. 4 (2015) 8–11.
[33] D. Shin et al., Science 314 (2006) 1607–1609.
[34] L.J. Holt, A.N. Krutchinsky, D.O. Morgan, Nature 454 (2008) 353–357.
[35] Y. Yang et al., Cell 146 (2011) 992–1003.
[36] J.W. Ramos, Int. J. Biochem. Cell Biol. 40 (2008) 2707–2719.
[37] B. Angelici et al., Cell Rep. 16 (2016) 2525–2537.
[38] N.A. Gormley et al., Biochemistry 35 (1996) 5083–5092.
[39] S. Knecht et al., J. Mol. Recognit. 22 (2009) 270–279.
[40] M.M. Kämpf et al., Adv. Funct. Mater. 20 (2010) 2534–2538.
[41] H.J. Wagner et al., Data Brief (2018).
[42] T.S. Thompson, D.K. Noot, J.D. Kendall, Food Addit. Contam. Part A 27 (2010) 1104–1111.
[43] A.A.K. Nielsen et al., Science 352 (2016). aac7341-1–aac7341-11.
[44] B.H. Weinberg et al., Nat. Biotechnol. 35 (2017) 453–462.
[45] W.L. Staudenbauer, E. Orr, Nucleic Acids Res. 9 (1981) 3589–3603.
[46] M. Ehrbar et al., Nat. Mater. 7 (2008) 800–804.